Spectral sideband produced by a hemispherical concave multilayer on the African shield-bug *Calidea panaethiopica* (Scutelleridae)

Jean Pol Vigneron,[1,*] Moussa Ouedraogo,[2] Jean-François Colomer,[1] and Marie Rassart[1]
[1]*Département de Physique, Facultés Universitaires Notre-Dame de la Paix, 61 rue de Bruxelles, B-5000 Namur, Belgium*
[2]*Centre National de la Recherche Scientifique et Technologique (CNRST), 03 BP 7047, Ouagadougou 03, Burkina Faso*
(Received 7 September 2008; revised manuscript received 7 January 2009; published 9 February 2009)

The African shield-backed bug *Calidea panaethiopica* is a very colorful insect which produces a range of iridescent yellow, green, and blue reflections. The cuticle of the dorsal side of the insect, on the shield, the prothorax and part of the head, is pricked of uniformly distributed hemispherical hollow cavities a few tens micrometers deep. Under normal illumination and viewing the insect's muffin-tin shaped surface gives rise to two distinct colors: a yellow spot arising from the bottom of the well and a blue annular cloud that appears to float around the yellow spot. This effect is explained by multiple reflections on a hemispherical Bragg mirror with a mesoscopic curvature. A multiscale computing methodology was found to be needed to evaluate the reflection spectrum for such a curved multilayer. This multiscale approach is very general and should be useful for dealing with visual effects in many natural and artificial systems.

DOI: 10.1103/PhysRevE.79.021907 PACS number(s): 42.66.−p, 42.70.Qs, 42.81.Qb

I. INTRODUCTION

Color mixing, such as producing green by simultaneously reflect yellow and blue, is not rare in nature [1]. The inappropriately named [2] "blue frog" (*Litoria caerulea*) [3], native to Australia and southern New Guinea, appears green as a result of blue Tyndall scattering and selective absorption by yellow pigments. In butterflies, color mixing can occur by pointillism, as in the case of the pea-green coloration of the ventral side of the Brazilian butterfly *Cyanophrys remus* [4]. Its yellow-green ventral color is due to the presence, in each scale, of a photonic polycrystal where the grains, assuming different orientations, produce yellow and blue-green incoherent reflections.

Another example of much interest is provided by the Indonesian male butterfly *Papilio palinurus*, where the dual colors, yellow and blue, are produced by a large (4–6 μm in diameter), nearly hemispherical cavity, aligned on some of the scales. As described by Vukusic *et al.* [5], the surface of this cavity is a multilayer specifically reflecting yellow under normal incidence, and—by iridescence [6,7] (the change of color with varying incidence and emergence angles)—blue at incidences close to 45°. The mixing of blue and yellow is again perceived as green, though the reflectance spectrum contains two clearly differentiated components, near 480 and 580 nm. The geometric deformation of a multilayer that produces this kind of stimulus synthesis is probably not rare in natural photonic structures, as it has also been reported by Berthier *et al.* in a few species [8], including on the elytra of the tiger beetle *Cicindela campestris*. In the present paper, we describe the same effect on a completely different type of insect and on a different length scale.

The insect we investigate in the present work is named *Calidea panaethiopica* (Kirkaldy 1909). It belongs to the family of Scutelleridae, a cosmopolitan category of bugs, comprising about 80 genera and over 450 species [9]. This family is commonly known to gather the "shield-backed bugs," so-called because the dorsal part of their abdomen and their wings are covered with a single piece of cuticular material with the shape of a heraldic shield (contrasting beetles, with separated elytra). *Calidea panaethiopica* has a pair of wings which fit unfolded under the shield when the animal is resting, and can be deployed laterally for flight. As with other shield bugs, adult *Calidea panaethiopica* have sucking mouth parts, and feed on the juice of seeds, leaves, and stems of a variety of herbaceous plants, trees, and shrubs.

A dry specimen of adult *Calidea panaethiopica* is shown in Fig. 1. Its body displays a complex color pattern, a diffusive reddish-brown underside, with bright blue-green iridescent lateral stripes. On the dorsal side, black bands are laid across iridescent areas appearing yellow, green or blue, according to the viewing angle. These striped, colored, surfaces cover the dorsal shield, the prothorax and the head. The cuticular surface is gleaming, but rough, due to the presence of a myriad of small dips.

The present paper will focus on the visual appearance produced by these hemispherical dips, distributed on the dorsal side of the insect. The optical properties of such a surface

FIG. 1. (Color online) Adult *Calidea panaethiopica* found in Burkina Faso, Africa. The complex pattern of colors of this insect, of the family of Scutelleridae (shield-backed bug), contains iridescent parts which, according to the viewing and illumination angles appear with a range of yellows, greens, and blues.

*jean-pol.vigneron@fundp. ac.be

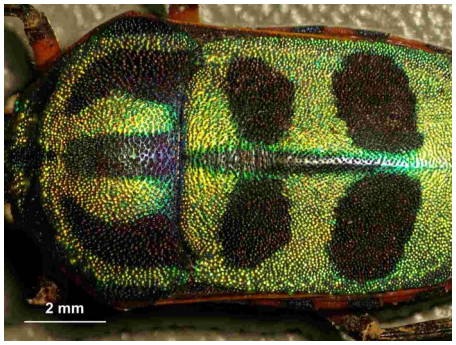

FIG. 2. (Color online) A microscopic overview of the surface of the shield of *Calidea panaethiopica*. Note the distribution of hemispherical dips, separated by bumpy areas.

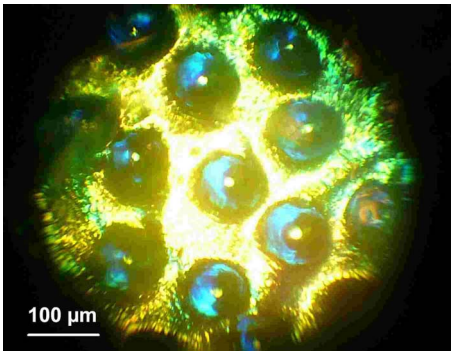

FIG. 3. (Color online) Optical microscope image of the surface of the cuticle of *Calidea panaethiopica*, in reflection mode, using a lateral (45°) illumination (source on the right). The surface appears to be imprinted by hemispherical dips which appear as blue disks, with a yellow spot at the center. The flat surface between the wells is brightly yellow.

will be examined (Sec. III) and the detailed structure of the dips will be studied with resolutions ranging from about 10 nm (using electron microscopy) to millimeters (Sec. IV).

This analysis will suggest that all length scales contribute to the formation of reflectance spectrum. A multiscale methodology will then be introduced to describe the color mixing which occurs when the shape of a nanoscopic iridescent reflector is controlled by a mesoscopic deformation of its substrate (see Sec. V and the Appendix).

II. OBTAINING SAMPLES

The specimens under study were collected in Burkina Faso and stored for several years at the "Centre National de la Recherche Scientifique et Technique" (CNRST, Burkina Faso) before being used for this study. The long period of dry storage did not alter the insect's appearance.

III. OPTICAL PROPERTIES OF THE IRIDESCENT SURFACE

The optical imaging and measurements were carried out on a shield, easily detached from one of the dry specimens. It was examined, as is, through an optical microscope. When measuring the optical reflectance, the shield was first glued and pressed onto a glass plate for an easier definition of the incidence and emergence angles.

A. Optical microscopy

At a moderate magnification, the iridescent surface of the cuticle does not appear to be planar. To the naked eye, the insects lacks the metallic aspect found on some other tropical "jewel beetles." Figure 2 shows the roughness of the surfaces between two neighboring black stripes on the dorsal shield. As Fig. 3 shows, this roughness is caused by hemispherical dips, all very close to 88 μm in diameter, with an average distance between the centers of 133 μm. The smooth surface between the hemispherical dips is not exactly flat, but bumpy, with a corrugation the height of which can be estimated to 10–20 μm.

When illuminated by a source very slightly displaced from the cuticle normal, this corrugated surface shows a series of dark disks with a yellow central spot surrounded by an annular cloud of blue light. These two coloration components will now be quantified in reflectance measurements.

B. Reflectance spectroscopy

An Avaspec 2048/2 fiber-optic spectrophotometer with a combined equilibrated halogen-deuterium source covering the (human) visible spectral region was used for the measurements. We will only report specular "backscattering" measurements at a near-normal incidence, though larger angles have also been explored, without providing much more information. The reflected intensity is compared to the intensity scattered from a standard diffusive white polytetrafluoroethylene reference (Avaspec). With this normalization, the reflected intensity is usually referred to as a "reflection factor," expressed in %. This quantity is not bound to be less than 100%.

The reflection factor of the shield under 15° of incidence is shown in Fig. 4. The main reflection is yellow-green, with a broad maximum near 560 nm. On the short-wavelength

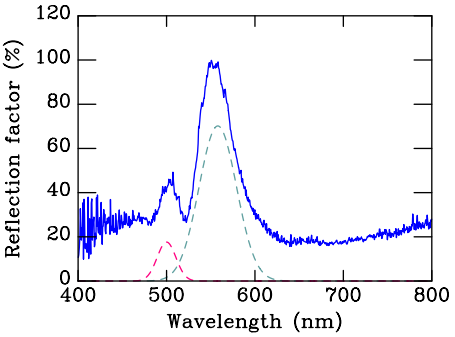

FIG. 4. (Color online) Experimental reflection factor of the shield of *Calidea panaethiopica* under normal incidence. The main reflection is yellow, with a broad maximum near 560 nm. A blue-green side band, near 500 nm also appears clearly. The dashed lines are separated components of a best-fit decomposition of the observed spectrum as a double Gaussian, showing the relative importance of the sideband.

side of this band, a weaker sideband appears, near 500 nm. These contributions are identified by color science [10] as "yellow green" and "bluish green," respectively. These contributions can be better appreciated by empirically best fitting two symmetric lines (in this case, Gaussian) to the measured spectrum, removing a constant background. This is shown as dotted lines on Fig. 4. The sideband contribution represent less than 10% of the main yellow band.

Determining the origin of these two spectral components requires a multiscale analysis, which must take into account the local nanoscopic structure and the distribution of surface orientations associated with the long-range cuticle corrugation. The next sections will address these questions in detail.

IV. NANOMORPHOLOGY

For this investigation, small pieces of shields were cut from the cuticle of *Calidea panaethiopica* and fractured at very low temperature, in liquid nitrogen. The resulting samples were mounted upright (so that their cross section can be scanned) on a primary sample holder. This holder was then sticked to a larger holder fitting the microscope in use with carbon tape. Metallization was avoided to ensure getting access to the real sample surface. Samples were investigated in a JEOL 7500F microscope. This field-emission scanning electron microscope (FESEM) permits to characterize nonconductive samples using a "gentle beam" mode[©JEOL] with enough resolution to process our natural samples while avoiding charging effects.

The cross section at the bottom of one of the dips is shown in Fig. 5. The image shows 15 periods of a Bragg mirror based on a double layer, slightly curved to follow the shape of the hemispherical dip. Each period is an assembly of two layers: a solid slab of bulk chitin and a layer of densely packed short, upright, chitin pillars separated by air. Both layers have a thickness of 95 nm. The second layer has a lateral corrugation, but the lateral period (on the average, 85 nm) is too short to produce diffraction in the wavelength range of interest. The layer behaves as a zero-order grating that provides the refractive index contrasts needed to produce the light stop band. The structured layer provides an effective refractive index intermediate (given the chitin filling fraction observed in FESEM) between chitin and air, close to 1.4, based on the widely accepted value of 1.56 for the refractive index of chitin. This value, recommended long ago [11], has since been used in a number of successful simulations. It is also consistent with a more detailed report of the optical properties of chitin [12]. Absorption, dispersion and anisotropy is however neglected in the present model.

On the basis of these observations, it is readily possible to estimate the wavelength that should be selected by reflection. The infinite Bragg mirror approximation [6], with a period length $a=190$ nm and a global effective refractive index of $\bar{n}=1.5$, predicts a dominant reflected wavelength λ of

$$\lambda = 2\bar{n}a = 570 \text{ nm}. \tag{1}$$

This crude estimation is consistent with the observation of the main reflection component in the yellow-green spectral range. We conclude that the surface multilayer is a Bragg mirror which, under normal incidence, selects a band of electromagnetic waves producing a yellow-green color.

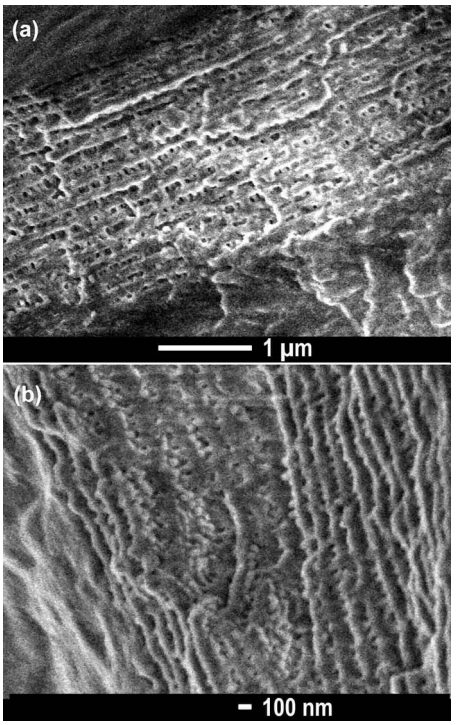

FIG. 5. (a) Scanning electron microscope view of the cuticle cross section near the bottom of a dip. The outer structure is a multilayer stacking groups of two different layers. The first is a layer 95-nm thick made of solid chitin. The second, of the same thickness, is a mixed structure, with chitin pillars standing in air between two solid slabs. (b) This more normal view reveal the pillars, which act as spacers for the bulk layers.

The second, weaker component detected in the spectrum, for wavelengths around 500 nm, can arise from the iridescence of the same Bragg mirror. At an angle γ with the local normal, the reflected wavelength is shifted by iridescence to the shorter-wavelength value

$$\lambda(\gamma) = 2a\sqrt{\bar{n}^2 - \sin^2\gamma} \tag{2}$$

which, in the case of this multilayer and with a local incidence angle $\gamma=37.5°$ (this corresponds to a global incidence of $\theta=15°$ off the normal to the average cuticle surface), turns out to be in the blue:

$$\lambda(37.5^o) = 521 \text{ nm}. \tag{3}$$

On this basis, the sideband production is easily understood, when referring to the diagram in Fig. 6. This diagram shows a cut through the diameter of the hemispherical dip, and through the outer multilayer. For rays falling under a global near-normal ($\theta=15°$) incidence along the spherical dip vertical axis, the impact is at the well bottom, and the local incidence γ is just the global angle θ, measured from the vertical cuticle normal. This results in the scattering of some yellow light, with a dominant wavelength near 561 nm. The same is true for light rays impinging on the nearly flat areas

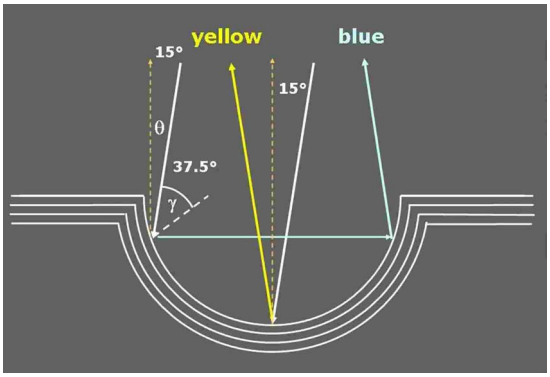

FIG. 6. (Color online) Suggested mechanism for the production of the blue-green sideband, using a curved iridescent Brag mirror. The description of this mechanism requires a multiscale approach of the reflection process, mixing ray tracing and wave optics. In a hemispherical dip, the blue sideband occurs after two reflections under a local incidence angle of $\gamma=37.5°$, when the incident ray makes an angle $\theta=15°$ with the (vertical) global normal.

between the dips. For light rays touching the sphere interior under $\gamma=37.5°$ from the local normal, the reflected light is blue, and stays blue after a second, symmetric reflection. The fact that this blue reflected light is much weaker than the yellow primary beam is essentially a consequence of the double reflection filtering. The blue sideband, which needs two reflections, cannot be very intense.

In order to quantitatively assess the relative strength of the sideband compared to the primary reflection, a multiscale analysis of the reflected intensity is needed. Applying this analysis to the hemispherical multilayer is the subject of the next section. The technical aspects of the multiscale computing approach used here are too intricate to be developed at this point. However, all needed ideas to develop this methodology are detailed in the Appendix, at the end of this paper.

V. MULTISCALE SCATTERING FROM A HEMISPHERICAL CAVITY

The geometry of the cuticle surface on the shield of *Calidea panaethiopica* can be approximated by the repetition of a hemispherical dip over the nodes of a square lattice. The unit cell of this two-dimensional lattice is shown in Fig. 7. The square lattice parameter is $a=133$ μm (the average distance between neighboring-dips centers) and the dip radius is $r=44$ μm. The triangulation of this surface produced 352 triangular sample-surface elements per unit cell.

The multiscale approach described in the appendix has been used to simulate the illumination, under 15° of incidence, of the cell shown in Fig. 7. The source at 10 cm was given an hexagonal shape, with a radius of 200 μm. It emits a parallel (unfocused) beam towards the central period. The detector, also at 10 cm and hexagonal, is mounted in a specular setup and is given a wide aperture (5 cm). The spectrum in Fig. 8 (solid line) collects the intensities from all detector elements. Polarization effects were discarded in this computation.

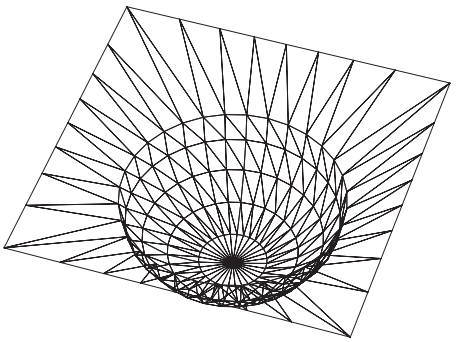

FIG. 7. One period of the model surface to represent the cuticle from the shield of *Calidea panaethiopica*. This surface element, cut into triangles, experiences a light-ray bombardment from an hexagonal source, with an axis at 15° with the vertical z direction. The detector is in a specular setup.

The multilayer which uniformly covers the whole surface contains 12 layers, all 90 nm thick, alternating the refractive indexes 1.56 and 1.4. The outer refractive index is 1.0, while the inner refractive index (substrate) is set to 1.56. This flat-layers structure copies the characteristics of the exocuticle of *Calidea panaethiopica*, as described earlier.

The main contribution near 530 nm can be readily identified as a band generated near the normal local and global incidences. In view of the idealization of the multilayer model, the slight discrepancy is not significant and this result confirms that the observed multilayer is responsible for the bright yellow reflection observed experimentally. The calculation also gives another contribution, appearing near 460 nm, which fits well (including intensity) the double-reflection scattering events described earlier. The oscillations shown on the calculated spectrum arise from interferences in the thick (12×90 nm≈1 μm) layer of effective photonic-crystal material. These do not show up clearly in the measured spectrum partly because the incident source was weak in this frequency range, and also, presumably, because the interface with the substrate is far from perfect. In the resulting computed spectrum, these oscillations build up from the short-range treatment of the multiscale geometry, while the

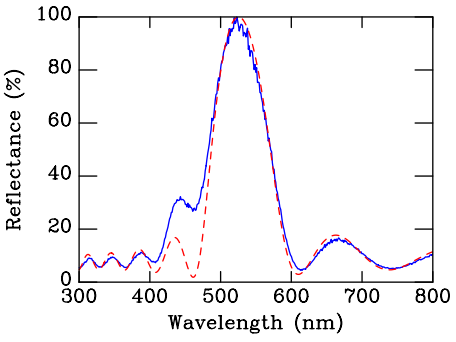

FIG. 8. (Color online) Computed normal backscattering by the hemispherical multilayer shown in Fig. 7 (solid line). The source is large enough to direct light rays to the whole two-dimensional period. The source and detector axis are set up in a specular geometry, with an average angle of incidence of 15°. The dashed line is the reflection factor on a flat multilayer.

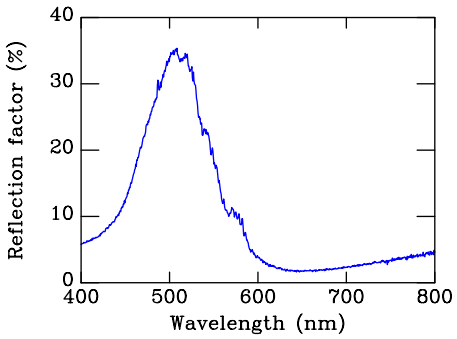

FIG. 9. (Color online) The scattering spectrum, for a specular geometry and an angle of incidence $\theta=45°$. The iridescence produces a shift of the main reflection (flat multilayer) to about 500 nm, correctly predicted by Eq. (2). The sideband is now on the long-wavelength side of peak, as expected from Eq. (5).

remaining noise is associated with the finite number of ray-tracing steps used to handle the long-range part of the geometry.

One of the remarkable properties of the doubly reflected beam is the "reverse" iridescence: the relationship between the local incidence γ and the global incidence θ is simply (see Fig. 6)

$$\gamma = \frac{\pi}{4} - \frac{\theta}{2}. \tag{4}$$

The double-reflection peak then changes with the global incidence angle θ as given here:

$$\lambda = 2a\sqrt{\frac{2\bar{n}^2 - 1}{2} + \frac{1}{2}\sin\theta}. \tag{5}$$

This means that the selected wavelength *increases* when the global angle of incidence θ increases. The reflected wavelength varies from $\lambda = 2a\sqrt{\bar{n}^2 - 1/2}$ at normal incidence to $\lambda = 2a\bar{n}$ near grazing incidence.

The measured specular spectrum shown in Fig. 9 was obtained by setting the incident beam at an angle of 45° with respect to the outer surface of the cuticle. In this configuration, the main peak should be blueshifted to $\lambda = 502.6$ nm, according to Eq. (2), while the side band can be estimated to lie near $\lambda = 551$ nm according to Eq. (5). This means that the main peak and the sideband crossed on the wavelength axis, as the incident angle was increased. The sideband observed on Fig. 9 is indeed on the red side of the main peak, at a wavelength somewhat higher than the theoretically predicted value. The small discrepancy—and the width and weak structuring of the sideband—is likely related to irregularities in the spherical shape of the cavities and to the fact that, under a larger incidence, the illuminated area contains several dips.

A light ray impinging on the dip under an incidence such as 15° or 45° will generate quite a number of scattered light rays, in addition to those represented in Fig. 6. Some of them undergo, in three dimensions, more than two reflections before exiting the dip. All these cases are included in a Monte Carlo calculation. However, when illuminating the dip with a highly directional beam and selecting the emergent rays with the aperture of a narrow light detector, in the specular geometry, drastically reduces the number of relevant paths that produce the spectrum. In this case, only paths very close to the symmetric" trajectories shown in Fig. 6 have a real importance. The discarded paths, however, will be important when viewing the insect's tegument under an extended, diffuse light source, releasing the specularity constraint.

VI. CONCLUSION

The shield-backed bug *Calidea panaethiopica* has developed a structurally colored cuticle on a deeply corrugated surface. Locally, this geometry allows for a bright yellow reflection at normal incidence. Iridescence, however, plays an important role in the visual appearance of this insect.

One of the most interesting characteristics of the cuticle geometry is the presence of hemispherical dips which generate observable blue intensity by a process involving two filtering reflections. This effect is probably too weak to have any biological significance, so that it is difficult to associate the presence of these dips on the insect's cuticle surface to any visual display function.

However, the study of this specific surface brought us two interesting outcomes: (1) it drove interest for developing a new multiscale methodology to approach the multiscale scattering by curved surfaces supporting a Bragg mirror. This development is basic to the study of many *natural* coloring structures. (2) It provides biomimetic inspiration for artificially developing surfaces with a new type of iridescence, involving a long-range double reflection. The "anomalous" shift of the selected color with the angle of incidence makes this new type of iridescence particularly interesting.

The multiscale approach of visual effects is a very important development, in view of its ability to help in the analysis of structural coloration. Iridescence provides a strong relationship between the overall shape of the reflecting surface and the spectrum it generates in a well-defined direction. The bidirectional reflectance distribution function (BRDF) on ordinary—pigmentary—surfaces is primarily influenced by the surface geometry because the scattered light *intensity* depends on the incidence direction. With structural colors, the change of reflected *hue* with the illumination direction adds further tuning possibilities. This can be an interesting opportunity to develop visual effects that have not been met before.

ACKNOWLEDGMENTS

The study was partly supported by the EU through FP6 BIOPHOT (NEST/Pathfinder) 012915 project and by the European Regional Development Fund (ERDF). The authors acknowledge the use of Namur Interuniversity Scientific Computing Facility (Namur-ISCF), a common project between the FNRS and the University of Namur (Belgium). M.R. and J.-F. C. were supported by the Belgian National Fund for Scientific Research (F.R.S.-FNRS).

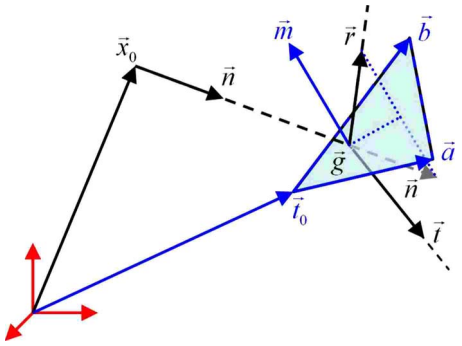

FIG. 10. (Color online) Geometry elements for the ray-tracing procedure. The triangle defined by the vectors $\vec{a}$ and $\vec{b}$ is hit at the point $\vec{g}$ by the ray with origin $\vec{x}_0$ and direction $\vec{n}$. It will be replaced by the reflected and transmitted rays, with respective directions $\vec{r}$ and $\vec{t}$.

APPENDIX: MULTISCALE APPROACH OF SCATTERING BY AN IRIDESCENT SURFACE

Though built from a finite number of layers, a Bragg mirror can be approximately described as an *infinite* one-dimensional photonic crystal. The occurrence of gaps leads to total reflection in a limited range of wavelengths and to iridescence, defined as the shift of the dominant reflected wavelength with a varying angle of incidence. A curved surface covered with a Bragg mirror not only scatters the reflected light in many directions, but also produces an incoherent mixing of colors in each of these directions. The spectral contents of the scattered light is not conceptually difficult to assess, because light propagation in structured materials is known from Maxwell's equations for nanoscale scattering, and by ray tracing (geometrical optics) for larger scales. Technical difficulties remain, however, when both scales must be accounted for in the same system, as in many natural or artificial structural coloration devices. In this section, we describe a procedure to couple coherent reflection to the incoherent scattering due to the long-range shape of the surface supporting this multilayer. Because of the variety of effects and shapes, a general approach is, by necessity, computational.

We start from a "forward" ray-tracing scheme which describes light propagation from a source to a detector. Four basic objects are defined as the "light ray," the "sample-surface element," the "light-source element," and the "detector element." Object-oriented computing languages are probably the best way to construct such objects in a computer code.

A "light ray" has (see Fig. 10) an origin in space $\vec{x}_0$ and a normalized direction of propagation $\vec{n}$. It also carries a normalized linear-polarization vector $\vec{\eta}$, constrained to be perpendicular to the propagation direction. A specific wavelength λ, an intensity i_0 and a "collapsing" intensity level i_c, which–when reached by a decreasing intensity–forces the ray to be suppressed.

A "surface element" is specified by its geometric parameters: two vectors $\vec{a}$ and $\vec{b}$ which define the two sides of a three-dimensional triangle attached to a common origin $\vec{t}_0$. The surface has an "inside" and an "outside," usually (but not mandatorily) with the physical meaning of bounding an object. A normalized vector $\vec{m}$, perpendicular to $\vec{a}$ and $\vec{b}$ indicates the direction of the "outside." Further information on the multilayer, part of the sample surface element, controls the reflection and transmission. This is (1) the number of layers n_l, (2) a list of thicknesses d_i, $i=1,\ldots,n_l$, and corresponding dielectric functions ε_i, $i=1,\ldots,n_l$, labeled in a well-defined order, from the inside to the outside, i.e., along the normal $\vec{m}$. The dielectric function should, in the most elaborate cases, be adjusted according to the wavelength of the incident light ray, and redefined for each impact of a ray, if dispersion is important. The dielectric constant of the "inside" and "outside" media should also be associated. In principle, anisotropic materials can also be considered by replacing the dielectric constants by dielectric tensors.

A "light-source element" is also a triangle, with the same geometrical data as before, $\vec{t}_0$, $\vec{a}$, $\vec{b}$, and $\vec{m}$, but this time no multilayer is associated to it. Instead, a focal point $\vec{f}$ should be given, allowing one to determine whether the light rays emitted from a random point in the element should be focussed ($\vec{f}$ in the direction of the scatterer) or defocused ($\vec{f}$ behind the source, away from the sample surface). This will help define illumination conditions such as those encountered in microreflectometry. The polarization properties of the source can also be specified, by defining two unnormalized vectors orthogonal to each other, and orthogonal to the normal $\vec{m}$. Each emitted ray will be given a polarization vector which is a random linear combination of these two vectors. For nonpolarized sources, the two vectors have equal norm; for linearly polarized light, one of the vectors will be given a null length. Finally, the intensity i_0 and the collapsing intensity i_c to be transferred to the emitted rays are associated.

A "detector element" is also a triangle in the three-dimensional space, described by the vectors $\vec{t}_0$, $\vec{a}$, $\vec{b}$, and $\vec{m}$. This element carries a multichannel device: a set of n_λ intensities, initially set to zero, which cover the wavelength range from $\lambda_{\min}$ to $\lambda_{\max}$. When hit along a specific direction (determined by the normal $\vec{m}$) by a light ray of wavelength λ, the "detector element" destroys it, and adds its intensity to the appropriate spectral channel. A polarization detection capacity is also added by defining an "analyzer" axis direction and storing the intensities into separate polarized multichannels, according to Malus law, for polarizations parallel and orthogonal to this analyzer axis.

These objects being defined, a typical numerical experiment is organized as follows. The global sample surface is first defined, assembled from triangular surface elements; a light source is constructed, with—usually—several triangular elements; a detector is setup from elements carrying their own multichannel recorder (they can be integrated afterwards, but more detail on scattering directions might be needed). A list of light rays, initially empty, is prepared. A first light ray, emitted from a random point in a random triangular light-source element, is stored as a first item in the list of rays. The light-source characteristics provide the intensity, the collapsing level and the polarization to the ray, which is sent in a direction which contains the focus point.

When ready, the control is passed to the ray-tracing system.

The ray-tracing system is programmed to examine the topmost ray in the list and see whether this ray hits nothing (then suppressed), hits a detector element (then suppressed, while its intensity is recorded on the appropriate spectral channel of the element) or hit a sample surface element (in which case the ray is replaced in the list by its subsequent reflected and transmitted rays, with intensities and polarization calculated, assuming an unbounded multilayer mirror; when one of these new rays have an intensity lower than the collapsing level, it is not created). This ray-tracing loop is restarted continuously, until no ray remains in the list. Then, a new ray is launched and the whole process is repeated, building the spectrum in each detector element. Enough launches are needed (typically, one million) to reach a negligible level of noise in the result.

To determine whether a light ray $[\vec{x}_0,\vec{n}]$ will hit the surface of a triangle $[\vec{t}_0,\vec{a},\vec{b}]$ (see Fig. 10) requires finding the point $\vec{g}=\vec{x}_0+t\vec{n}$ which matches one of the points in the plane of the triangle, $\vec{p}=\vec{t}_0+u\vec{a}+v\vec{b}$. This means solving the set of three linear equations $u\vec{a}+v\vec{b}-t\vec{n}=\vec{x}_0-\vec{t}_0$ for the unknown quantities t, u, and v. For a hit to happen, the conditions $t \geqslant 0$, $0 \leqslant u < 1$, $0 \leqslant v < 1$, and $u+v<1$ should all be true.

Once a ray $[\vec{x}_0,\vec{n}]$ has hit a sample surface element $[\vec{t}_0,\vec{a},\vec{b},\vec{m}]$ at an interior point $\vec{g}$, the ray should be replaced by its reflected and transmitted successors. The reflected ray is $[\vec{g},\vec{r}]$, where

$$\vec{r}=\vec{n}-2(\vec{n}\cdot\vec{m})\vec{m}. \tag{A1}$$

In this expression, $\vec{n}$ and $\vec{m}$ are normalized vectors, while $\vec{r}$ should be normalized after evaluation. The transmitted ray $[\vec{g},\vec{t}]$ changes direction because of refraction. The new direction is subject to verify Snell's law. The incidence angle θ_{in} (positive and smaller than 90°) is given by the norm

$$\sin\theta_{\text{in}}=|\vec{n}\times\vec{m}|. \tag{A2}$$

and the transmitted light ray emerges at the refraction angle θ_{out} such that

$$\sin\theta_{\text{out}}=\sqrt{\frac{\varepsilon_{\text{in}}}{\varepsilon_{\text{out}}}}\sin\theta_{\text{in}}. \tag{A3}$$

Similarly, one easily finds that

$$\cos\theta_{\text{in}}=\vec{n}\cdot\vec{m} \tag{A4}$$

while

$$\cos\theta_{\text{out}}=\text{sign}[\cos(\theta_{\text{in}})]\sqrt{1-\sin^2\theta_{\text{out}}}. \tag{A5}$$

If real, this quantity defines the refracted beam direction as

$$\vec{t}=\cos(\theta_{\text{out}})\vec{n}+\sin(\theta_{\text{out}})\vec{u}, \tag{A6}$$

where

$$\vec{u}=\frac{\vec{n}-(\vec{n}\cdot\vec{m})\vec{m}}{|\vec{n}-(\vec{n}\cdot\vec{m})\vec{m}|} \tag{A7}$$

defines the plane of incidence, together with the normal $\vec{m}$. If the calculation of the expression 10 leads to an imaginary number, the reflection is total and there is no point computing the direction $\vec{t}$.

In these expressions, ε_{in} is the dielectric constant of the incident medium and ε_{out} is the dielectric constant of the emergent medium. Their values are stored with the surface element properties, but depend on the direction of incidence $\vec{n}$, relative to the surface vector $\vec{m}$. Note that the new direction vector $\vec{t}=\vec{t}_{\parallel}+\vec{t}_{\perp}$ is readily normalized. The transmitted and reflected intensities are calculated by a standard multilayer algorithm (see, for instance, Ref. [13]), after decomposition of the incident polarization into s and p contributions.

This approach uses ray tracing for that part of the problem where the scale is much larger than the wavelength and Maxwell's equations when the ray hits a local Bragg mirror. This hierarchical approach is very efficient, especially on multinodes parallel computers: each ray launched from the source generates a computation independent of that performed for all other rays, so that the task can easily be distributed among available computers for earlier termination.

Note that the methodology introduced here, by varying the incidence (source) and emergence (detector) directions allows to calculate the full bidirectional reflectance distribution function of the multiscale surface. In fact, the approach described in the present section, arising from the particular study of the complex cuticle surface of *Calidea panaethiopica*, should be universally useful for the description of multiscale realistic structures, not only for structurally colored natural surfaces, but also for artificially developed iridescent objects.

[1] D. L. Fox, *Animal Biochromes and Structural Colours* (University of California Press, Berkeley, 1976).

[2] A. Parker, *Seven Deadly Colours. The Genius of Nature's Palette and How it Eluded Darwin* (Free Press, Simon & Schuster, London, 2005).

[3] J. Walls, *Fantastic Frogs* (T.F.H. Publications, Neptune City, NJ, 1995).

[4] K. Kertész, Z. Bálint, Z. Vértesy, G. I. Márk, V. Lousse, J. P. Vigneron, M. Rassart, and L. P. Biró, Phys. Rev. E **74**, 021922 (2006).

[5] P. Vukusic, J. R. Sambles, and C. R. Lawrence, Nature (London) **404**, 457 (2000).

[6] J. Vigneron and V. Lousse, Proc. SPIE **6128**, 61281G (2006).

[7] J. P. Vigneron, M. Rassart, C. Vandenbem, V. Lousse, O. Deparis, L. P. Biró, D. Dedouaire, A. Cornet, and P. Defrance, Phys. Rev. E **73**, 041905 (2006).

[8] S. Berthier, J. Boulenguez, and Z. Bálint, Appl. Phys. A: Mater. Sci. Process. **86**, 123 (2007).

[9] R. Schuh and J. Slater, *True Bugs of the World (Hemiptera:*

Heteroptera). Classification and Natural History (Cornell University Press, Ithaca, 1995).

[10] K. L. Kelly, *COLOR Universal Language and Dictionary of Names* (U.S. Department of Commerce, Washington, D.C., 1976).

[11] B. J. Sollas, Proc. R. Soc., London, Ser. B **79**, 474 (1907).

[12] S. Berthier, E. Charron, and A. D. Silva, Opt. Commun. **228**, 349 (2003).

[13] A. Dereux, J. P. Vigneron, P. Lambin, and A. A. Lucas, Phys. Rev. B **38**, 5438 (1988).